SCIENTIFIC REP♦RTS

OPEN

Hydrogenation-controlled phase transition on two-dimensional transition metal dichalcogenides and their unique physical and catalytic properties

Yuanju Qu[1,2], Hui Pan[1] & Chi Tat Kwok[1,2]

Two-dimensional (2D) transition metal dichalcogenides (TMDs) have been widely used from nanodevices to energy harvesting/storage because of their tunable physical and chemical properties. In this work, we systematically investigate the effects of hydrogenation on the structural, electronic, magnetic, and catalytic properties of 33 TMDs based on first-principles calculations. We find that the stable phases of TMD monolayers can transit from 1T to 2H phase or vice versa upon the hydrogenation. We show that the hydrogenation can switch their magnetic and electronic states accompanying with the phase transition. The hydrogenation can tune the magnetic states of TMDs among non-, ferro, para-, and antiferro-magnetism and their electronic states among semiconductor, metal, and half-metal. We further show that, out of 33 TMD monolayers, 2H-TiS$_2$ has impressive catalytic ability comparable to Pt in hydrogen evolution reaction in a wide range of hydrogen coverages. Our findings would shed the light on the multi-functional applications of TMDs.

Extensive attention has been drawn to two-dimensional (2D) transition metal dichacogenides (TMDs) because of their unique chemical, mechanical, electronic and magnetic properties, multi-functional applications in various fields of science and technology from spintronics, optoelectronics, sensors, catalysts to energy harvesting and storage[1–14], and easier fabrication[2,15–18]. Depending on the point-group symmetries (D$_{6h}$ and D$_{3d}$), these 2D monolayers with the formula of MX$_2$ can have 1T (Fig. 1a) or 2H phase (Fig. 1d)[2], where M is the transition metal element and X is a chalcogen element (S, Se, and Te). These 2D TMDs show rich physical and chemical properties and can be metallic, half-metallic, semiconducting, magnetic, and catalytic, which can be tuned by phase transition, composition engineering, surface functionalization, and external fields (strain and electrical field)[2,9,19–32]. For example, 2H MoS$_2$ and WS$_2$ monolayers are semiconductor, while their 1T phases are metallic[32–34]. Hydrogenated MoS$_2$ monolayer can be non-magnetic and ferromagnetic tuned by tensile strain[23]. Magnetic evolution from non-magnetism, to anti-ferromagnetism, via paramagnetism, then to ferromagnetism accompanying with electronic switching from semiconductor to metal, then to half-metal was achieved on VX$_2$ monolayers by hydrogenation and tensile strain[11,24]. Vanadium disulfide monolayer showed better catalytic performance than its selenides and tellurides counterparts[25] and tensile strain can enhance the ability dramatically[26]. The catalytic performance of MX$_2$ monolayers can be strongly improved by phase transition[30–38]. For example, the 1T phase MoS$_2$ and WS$_2$ nanosheet was proven to be more catalytically active in facilitating hydrogen production in electrolysis of water than their 2H counterpart, although 2H phase is more stable than its 1T phase[30]. Theoretically, it was reported that hydrogen-functionalization can trigger the 2H to 1T phase transition of MoS$_2$[28] and the catalytic activity of 1T-MoS$_2$ mainly arises from its affinity for binding H at the surface S sites[28,39–41]. Recently, 1T phase domains were formed in 2H-MX$_2$ monolayer by creating X vacancies and these 2H-1T mixed monolayer showed ferromagnetism[31]. Although oxidization is a simple way to create the vacancy for the phase

[1]Institute of Applied Physics and Materials Engineering, Faculty of Science and Technology, University of Macau, Macao SAR, P. R. China. [2]Department of Electromechanical Engineering, Faculty of Science and Technology, University of Macau, Macao SAR, P. R. China. Correspondence and requests for materials should be addressed to H.P. (email: huipan@umac.mo)
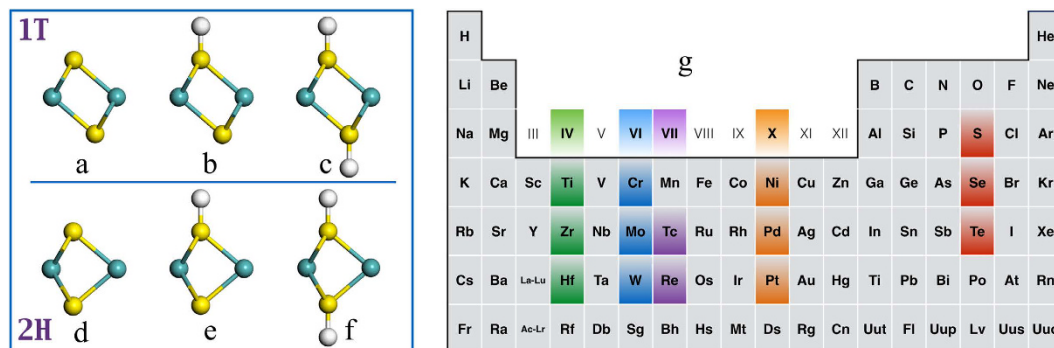
Figure 1. The representative unit cells of MX$_2$ monolayers in 1T phase: (**a**) MX$_2$-0HC, (**b**) MX$_2$-1HC, (**c**) MX$_2$-2HC. The representative structures of MX$_2$ monolayers unit cell in 2H phase: (**d**) MX$_2$-0HC, (**e**) MX$_2$-1HC, (**f**) MX$_2$-2HC. (**g**) the periodic table with highlighted transition metal atoms (M) and chalcogen atoms (X) considered in our calculations.
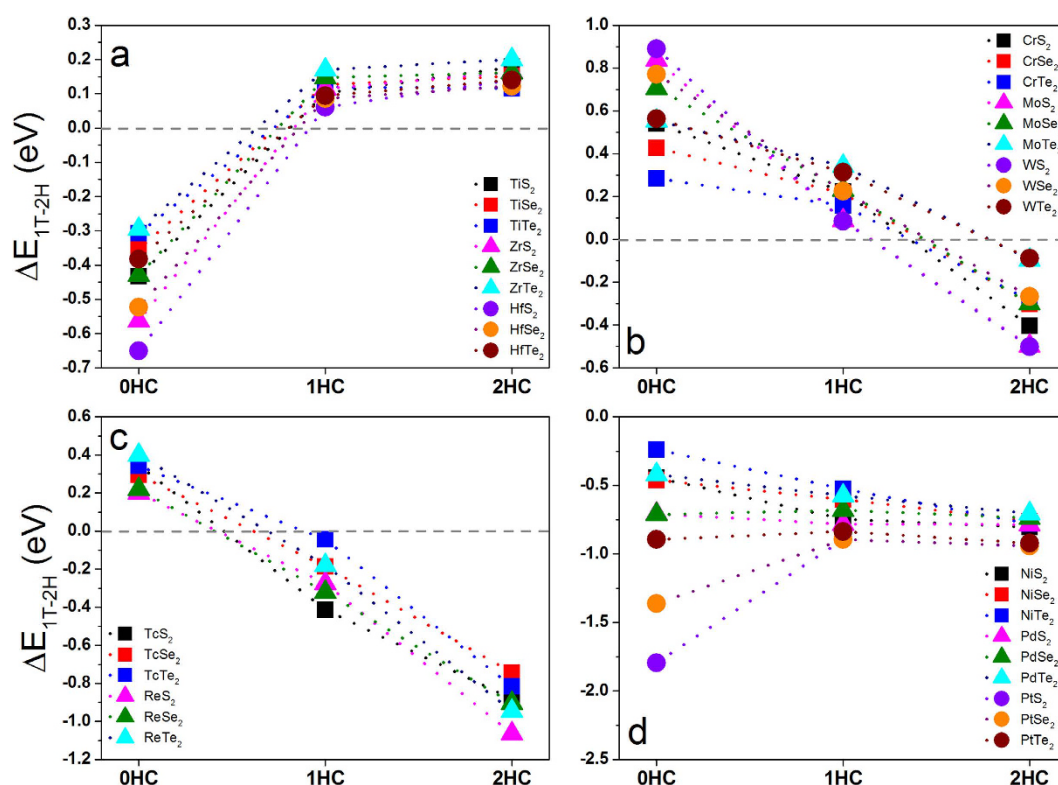
Figure 2. Calculated total energy differences between 1T and 2H phase of MX$_2$ monolayers with and without hydrogenation for metal elements from: (**a**) group IV: M = Ti, Zr & Hf, (**b**) group VI: M = Cr, Mo & W, (**c**) group VII: M = Tc & Re, (**d**) group X: M = Ni, Pd & Pt.

transition, it may also result in a lot of defects in the monolayers. In this work, we present a general method – hydrogenation – to realize the phase transition and tune the physical and chemical properties of 33 different MX$_2$ monolayers. We find that 1T and 2H phases can transform to each other upon hydrogenation, depending on the transition metal elements in MX$_2$ monolayers. Accompanying with the phase transition, their electronic properties switch among semiconducting, metallic, and half metallic, and magnetic ground states among nonmagnetic, ferromagnetic, paramagnetic and anti-ferromagnetic states. We further predict that TiS$_2$ monolayer in 2H phase shows effective catalytic performance for hydrogen evolution reaction in a wide range of hydrogen coverages with neutral thermal Gibbs free energies.

## Results and Discussion

Structural Properties.   In our calculations, we focus on 2D transitional metal dichalcogenides (MX$_2$) with M from group IV (Ti, Zr, and Hf), group VI (Cr, Mo, and W), group VII (Tc and Re), and group VIII (Ni, Pd,

Group IV	Condition	Stable Phase	a (Å)	X – M (Å)	Thickness (Å)	Group VI	Condition	Stable Phase	a (Å)	X – M (Å)	Thickness (Å)
TiS$_2$	0HC	1T	3.42	2.43	2.83	CrS$_2$	0HC	2H	3.04	2.29	2.94
	1HC	2H	3.47	2.45	4.18		1HC	2H	3.31	2.31	3.97
	2HC	2H	3.47	2.45	5.57		2HC	1T	3.43	2.34	5.25
TiSe$_2$	0HC	1T	3.54	2.56	3.10	CrSe$_2$	0HC	2H	3.21	2.43	3.15
	1HC	2H	3.64	2.58	4.50		1HC	2H	3.49	2.45	4.32
	2HC	2H	3.65	2.58	6.01		2HC	1T	3.67	2.48	5.62
TiTe$_2$	0HC	1T	3.75	2.78	3.49	CrTe$_2$	0HC	2H	3.47	2.64	3.42
	1HC	2H	3.93	2.79	4.97		1HC	2H	3.75	2.65	4.78
	2HC	2H	3.93	2.78	6.66		2HC	1T	3.99	2.66	6.10
ZrS$_2$	0HC	1T	3.69	2.57	2.89	MoS$_2$	0HC	2H	3.19	2.41	3.13
	1HC	2H	3.67	2.59	4.34		1HC	2H	3.22	2.44	4.57
	2HC	2H	3.60	2.59	5.83		2HC	1T	3.44	2.44	5.62
ZrSe$_2$	0HC	1T	3.80	2.70	3.16	MoSe$_2$	0HC	2H	3.32	2.54	3.34
	1HC	2H	3.82	2.71	4.66		1HC	2H	3.38	2.57	4.92
	2HC	2H	3.77	2.71	6.26		2HC	1T	3.65	2.58	5.99
ZrTe$_2$	0HC	1T	3.97	2.92	3.61	MoTe$_2$	0HC	2H	3.56	2.74	3.62
	1HC	2H	4.08	2.91	5.12		1HC	2H	3.90	2.74	4.86
	2HC	2H	4.04	2.90	6.87		2HC	1T	4.04	2.75	6.35
HfS$_2$	0HC	1T	3.64	2.55	2.89	WS$_2$	0HC	2H	3.19	2.42	3.14
	1HC	2H	3.62	2.56	4.32		1HC	2H	3.19	2.44	4.64
	2HC	2H	3.56	2.56	5.81		2HC	1T	3.40	2.44	5.68
HfSe$_2$	0HC	1T	3.77	2.68	3.14	WSe$_2$	0HC	2H	3.32	2.55	3.36
	1HC	2H	3.78	2.69	4.64		1HC	2H	3.34	2.57	4.99
	2HC	2H	3.70	2.68	6.30		2HC	1T	3.61	2.57	6.11
HfTe$_2$	0HC	1T	3.98	2.90	3.52	WTe$_2$	0HC	2H	3.56	2.74	3.63
	1HC	2H	4.04	2.89	5.11		1HC	2H	3.92	2.74	4.83
	2HC	2H	3.99	2.87	6.88		2HC	1T	4.06	2.76	6.40
Group VI						**Group X**					
TcS$_2$	0HC	2H	3.28	2.38	2.89	NiS$_2$	0HC	1T	3.36	2.26	2.32
	1HC	1T	3.68	2.41	3.60		1HC	1T	3.46	2.31	3.69
	2HC	1T	3.63	2.41	5.16		2HC	1T	3.63	2.37	4.96
TcSe$_2$	0HC	2H	3.42	2.51	3.10	NiSe$_2$	0HC	1T	3.54	2.39	2.48
	1HC	1T	3.85	2.53	3.93		1HC	1T	3.66	2.44	3.96
	2HC	1T	3.87	2.54	5.45		2HC	1T	3.81	2.49	5.37
TcTe$_2$	0HC	2H	3.67	2.69	3.33	NiTe$_2$	0HC	1T	3.79	2.58	2.73
	1HC	1T	4.05	2.70	4.41		1HC	1T	3.90	2.61	4.39
	2HC	1T	4.12	2.70	5.98		2HC	1T	4.05	2.66	5.99
ReS$_2$	0HC	2H	3.31	2.40	2.88	PdS$_2$	0HC	1T	3.55	2.40	2.48
	1HC	1T	3.32	2.42	4.35		1HC	1T	3.72	2.46	3.75
	2HC	1T	3.68	2.42	5.07		2HC	1T	3.94	2.53	4.96
ReSe$_2$	0HC	2H	3.46	2.52	3.08	PdSe$_2$	0HC	1T	3.74	2.52	2.61
	1HC	1T	3.86	2.54	3.93		1HC	1T	3.91	2.58	4.01
	2HC	1T	3.89	2.54	5.43		2HC	1T	4.10	2.64	5.36
ReTe$_2$	0HC	2H	3.71	2.70	3.30	PdTe$_2$	0HC	1T	4.03	2.70	2.75
	1HC	1T	4.09	2.71	4.37		1HC	1T	4.14	2.75	6.44
	2HC	1T	4.15	2.70	5.97		2HC	1T	4.31	2.80	6.01
						PtS$_2$	0HC	1T	3.58	2.40	2.46
							1HC	1T	3.93	2.58	3.99
							2HC	1T	4.14	2.64	5.29
						PtSe$_2$	0HC	1T	3.75	2.53	2.62
							1HC	1T	3.93	2.58	3.99
							2HC	1T	4.13	2.64	5.30
						PtTe$_2$	0HC	1T	4.02	2.71	2.78
							1HC	1T	4.15	2.74	4.44
							2HC	1T	4.30	2.79	6.02

Table 1. Stable phases and lattice parameters of MX$_2$ monolayers without hydrogenation (0HC), with one-surface full hydrogenation (1HC) and two-surface full hydrogenation.
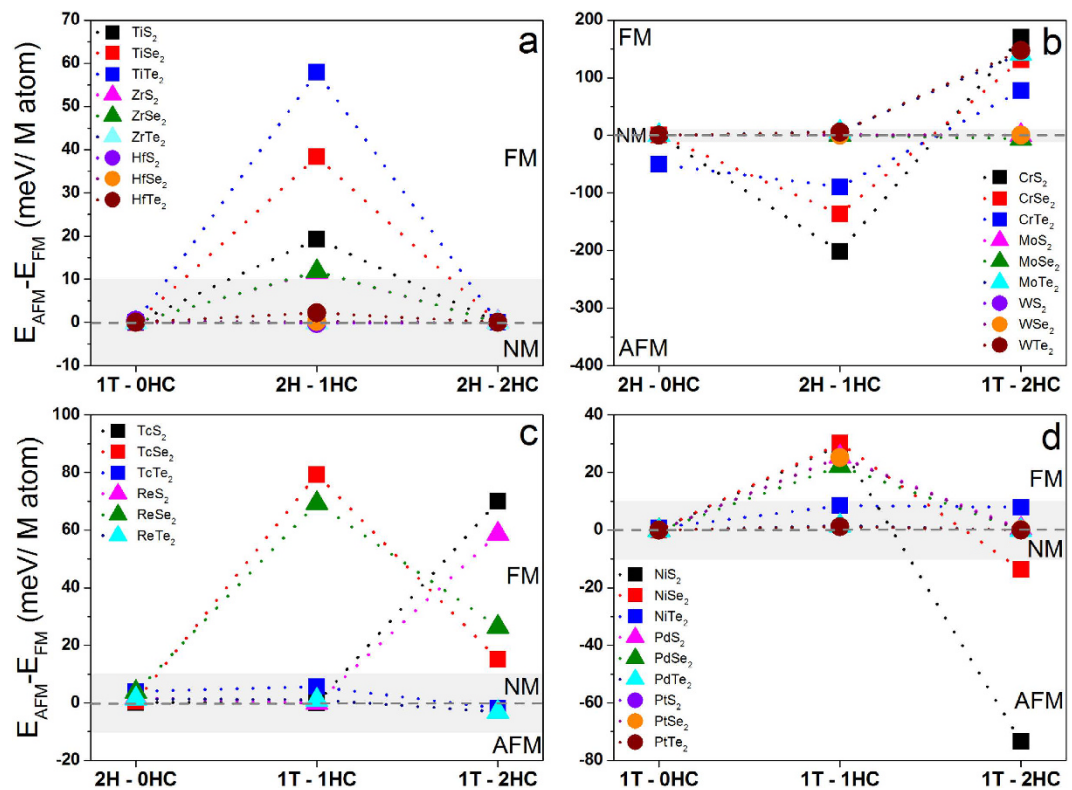
Figure 3. Calculated exchange energies between antiferromagnetic and ferromagnetic states of MX_2 monolayers with and without hydrogenation for metal elements from: (**a**) group IV: M = Ti, Zr & Hf, (**b**) group VI: M = Cr, Mo & W, (**c**) group VII: M = Tc & Re, (**d**) group X: M = Ni, Pd & Pt. The grey region indicates the non-magnetic states.
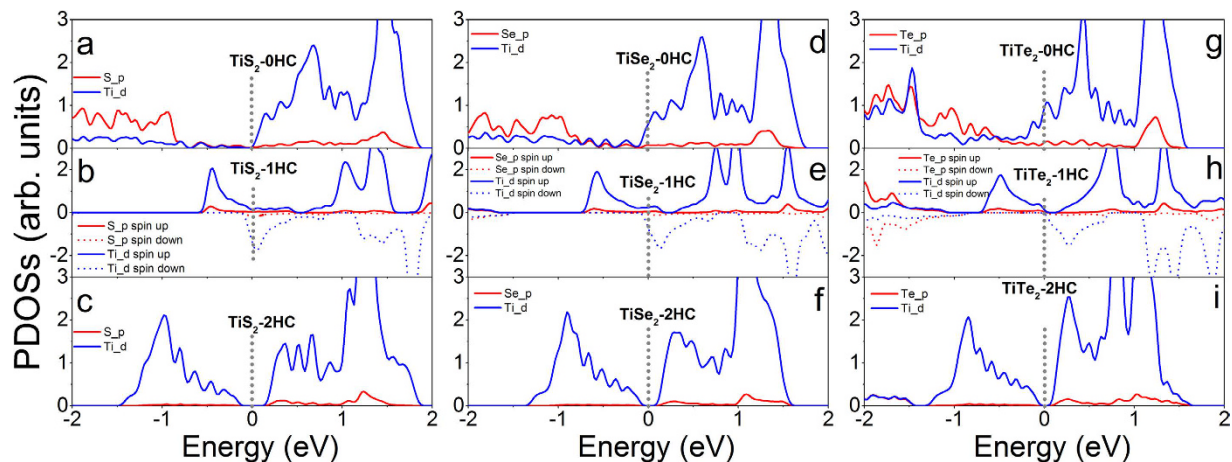
Figure 4. Calculated partial density of states of (**a**) TiS_2-0HC, (**b**) TiS_2-1HC, (**c**) TiS_2-2HC, (**d**) $TiSe_2$-0HC, (**e**) $TiSe_2$-1HC, (**f**) $TiSe_2$-2HC, (**g**) $TiTe_2$-0HC, (**h**) $TiTe_2$-1HC and (**i**) $TiTe_2$-2HC monolayers. The Fermi level is at 0 eV and indicated with gray dotted line.

and Pt), as shown in Fig. 1g. The hydrogenation of these TMDs is realized by putting hydrogen atoms directly on the tops of X atoms[41–44]. The MX_2 monolayers with and without hydrogenation is referred as MX_2-nHC, where n equals to 0 (no hydrogenation; Fig. 1a for 1T phase and Fig. 1d for 2H phase, respectively), 1 (one surface fully covered by hydrogen atoms; Fig. 1b for 1T phase and Fig. 1e for 2H phase, respectively), and 2 (two surfaces fully covered by hydrogen atoms; Fig. 1c,f for 1T and 2H phases, respectively). In order to identify the phase transition of 2D TMDs, all the MX_2 unit cells with and without hydrogenation in both 1T and 2H phases (Fig. 1) are firstly optimized to obtain the lattice parameters and formation energies. The phase transition can be identified by the energy differences (ΔE_{1T-2H}) between 1T and 2H phases of MX_2 as calculated from the following equation:

Group IV	Structure	Conductivity	Magnetic state	Magnetic moment of M atom (μ_B)	Magnetic moments of X atom & X atom with H (μ_B)	Curie Temperature (K)	Exchange Energy (meV)
TiS$_2$	1T-0HC	semiconductor	NM	—	—	—	0
	2H-1HC	semiconductor	FM	0.46	0.006 & 0.007	149	19
	2H-2HC	semiconductor	NM	—	—	—	0
TiSe$_2$	1T-0HC	metal	NM	—	—	—	0
	2H-1HC	semiconductor	FM	0.62	0.007 & 0.020	297	38
	2H-2HC	semiconductor	NM	—	—	—	0
TiTe$_2$	1T-0HC	metal	NM	—	—	—	0
	2H-1HC	semiconductor	FM	0.71	0.015 & 0.030	448	58
	2H-2HC	semiconductor	NM	—	—	—	0
ZrS$_2$	1T-0HC	semiconductor	NM	—	—	—	0
	2H-1HC	half-metal	FM	0.40	0.027 & 0.003	90	12
	2H-2HC	semiconductor	NM	—	—	—	0
ZrSe$_2$	1T-0HC	semiconductor	NM	—	—	—	0
	2H-1HC	half-metal	FM	0.42	0.013 & 0.002	91	12
	2H-2HC	semiconductor	NM	—	—	—	0
ZrTe$_2$	1T-0HC	metal	NM	—	—	—	0
	2H-1HC	semiconductor	NM	—	—	—	0
	2H-2HC	semiconductor	NM	—	—	—	0
HfS$_2$	1T-0HC	semiconductor	NM	—	—	—	0
	2H-1HC	metal	NM	—	—	—	0
	2H-2HC	semiconductor	NM	—	—	—	0
HfSe$_2$	1T-0HC	semiconductor	NM	—	—	—	0
	2H-1HC	semiconductor	NM	—	—	—	0
	2H-2HC	metal	NM	—	—	—	0
HfTe$_2$	1T-0HC	metal	NM	—	—	—	0
	2H-1HC	metal	NM	—	—	—	2
	2H-2HC	metal	NM	—	—	—	0

Table 2. Electronic, and magnetic ground states and magnetic moments of MX$_2$-nHC (n = 0, 1, and 2). Non-magnetism, ferromagnetism, and anti-ferromagnetism are denoted as NM, FM and AFM, respectively.
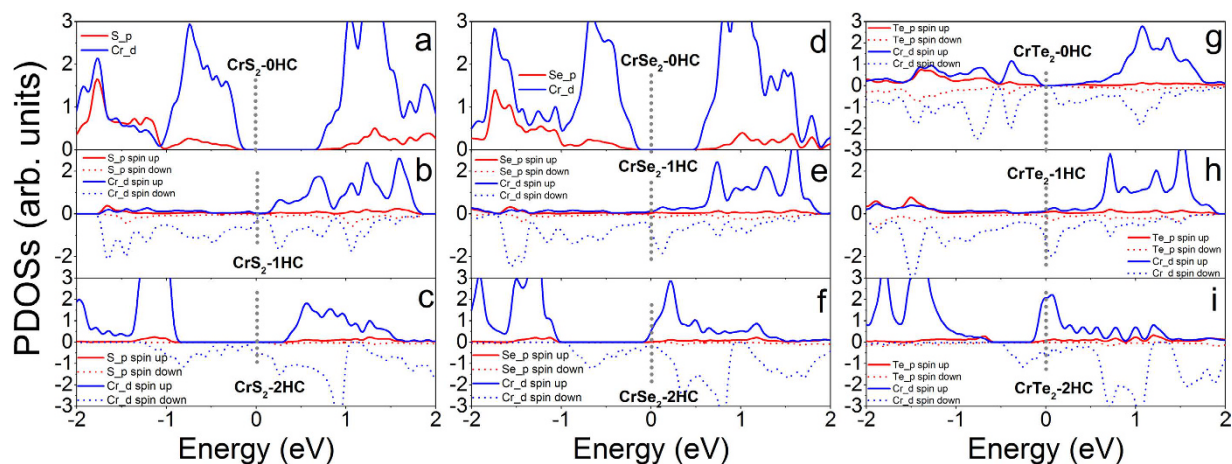
Figure 5. Calculated partial density of states of (**a**) CrS$_2$-0HC, (**b**) CrS$_2$-1HC, (**c**) CrS$_2$- 2HC, (**d**) CrSe$_2$-0HC, (**e**) CrSe$_2$-1HC, (**f**) CrSe$_2$-2HC, (**g**) CrTe$_2$-0HC, (**h**) CrTe$_2$-1HC and (**i**) CrTe$_2$-2HC monolayers. The Fermi level is at 0 eV and indicated with gray dotted line.

$$\Delta E_{1T-2H} = E_{1T} - E_{2H} \qquad (1)$$

where E_{1T} and E_{2H} are the total energies of a MX$_2$-nHC in 1T and 2H phases, respectively. If ΔE_{1T-2H} is negative, the 1T phase is more stable, otherwise 2H phase is more stable.

The negative ΔE_{1T-2H} shows that pure MX$_2$ monolayers with metal elements from group IV (M = Ti, Zr, and Hf) are stable in 1T phase (Fig. 2a). When their surfaces are hydrogenated, the 2H phases become stable, as

Group VI	Structure	Conductivity	Magnetic state	Magnetic moment of M atom (μ_B)	Magnetic moments of X atom & X atom with H (μ_B)	Curie Temperature (K)	Exchange Energy (meV)
CrS$_2$	2H-0HC	semiconductor	NM	—	—	—	0
	2H-1HC	metal	AFM	2.27	0.044 & 0.021	—	−202
	1T-2HC	half-metal	FM	1.97	0.018	1317	170
CrSe$_2$	2H-0HC	semiconductor	NM	—	—	—	0
	2H-1HC	metal	AFM	2.51	0.051 & 0.006	—	−137
	1T-2HC	metal	FM	2.11	0.039	1012	131
CrTe$_2$	2H-0HC	semiconductor	AFM	1.42	0.056	—	−50
	2H-1HC	metal	AFM	2.67	0.065 & 0.027	—	−90
	1T-2HC	metal	FM	2.62	0.089	596	77
MoS$_2$	2H-0HC	semiconductor	NM	—	—	—	0
	2H-1HC	semiconductor	NM	—	—	—	2
	1T-2HC	metal	NM	—	—	—	0
MoSe$_2$	2H-0HC	semiconductor	NM	—	—	—	0
	2H-1HC	semiconductor	NM	—	—	—	0
	1T-2HC	metal	PM	1.05	0.008	—	−6
MoTe$_2$	2H-0HC	semiconductor	NM	—	—	—	0
	2H-1HC	metal	NM	—	—	—	6
	1T-2HC	half-metal	FM	1.61	0.042	1096	12
WS$_2$	2H-0HC	semiconductor	NM	—	—	—	0
	2H-1HC	semiconductor	NM	—	—	—	0
	1T-2HC	metal	NM	—	—	—	0
WSe$_2$	2H-0HC	semiconductor	NM	—	—	—	0
	2H-1HC	semiconductor	NM	—	—	—	0
	1T-2HC	metal	NM	—	—	—	0
WTe$_2$	2H-0HC	semiconductor	NM	—	—	—	0
	2H-1HC	metal	NM	—	—	—	5
	1T-2HC	half-metal	FM	1.48	0.046	1137	147

Table 3.   Electronic, and magnetic ground states and magnetic moments of MX$_2$-nHC (n = 0, 1, and 2). Non-magnetism, paramagnetism, ferromagnetism, and anti-ferromagnetism are denoted as NM, PM, FM and AFM, respectively.

indicated by the positive ΔE_{1T-2H}. We also note that 1T transition metal disulfides (MS$_2$) are more stable than their selenides (MSe$_2$) and tellurides (MTe$_2$) with the same phase due to their larger negative energy differences. Differently, the MX$_2$ monolayers with the metal elements from group VI (M = Cr, Mo, and W) experience a phase transition of 2H → 2H → 1T as the hydrogenation progresses from 0HC, 1HC, to 2HC (Fig. 2b). Our result on MoS$_2$ is consistent with literatures[35–37]. From literatures[35–37], we also see that pure 2H-MoS$_2$ is more stable than pure 1T-MoS$_2$. As hydrogen coverage increasing, 1T-MoS$_2$ becomes stable[28]. If the metal element is from group VII, the MX$_2$ (M = Tc and Re) monolayers go through a phase transition of 2H → 1T → 1T as the hydrogenation increases from 0HC, 1HC, to 2HC (Fig. 2c). Totally different from the above three groups, all of the MX$_2$ monolayers with metal elements from group X (M = Ni, Pd, and Pt) are stable in 1T phase regardless of hydrogenation due to large negative energy differences. Our calculations show that pure MX$_2$ monolayers are stable in either 1T or 2H phase depending on the metal elements in their composition, and hydrogenation can trigger the phase transition from one to another effectively, except the MX$_2$ monolayers with M from group X. The MX$_2$ monolayers, where M atoms are in the same group, follow the same trend of phase transition under hydrogenation.

In the following discussion, the pure and hydrogenated MX$_2$ monolayers with the stable phases are investigated (Table 1 and Fig. 2). The optimized geometries show that the hydrogenation results more or less in the changes of their lattice constants. For MX$_2$ with M from group IV, their lattice constants (a) and the X-M bond length remain unchanged or slightly decrease under hydrogenation. For example, the lattice constant (a) are 3.47 Å for both TiS$_2$-1HC and TiS$_2$-2HC, slightly larger than that of TiS$_2$-0HC (3.42 Å). The lattice constant of pure TiS$_2$ monolayer is consistent with literature[45]. Normally, the thickness (the vertical distance between two chalcogen atoms) increases upon hydrogenation in all considered MX$_2$ systems. For MX$_2$ monolayers with M from group VI, VII, and X, both the lattice constant (a) and X-M bond length increase as hydrogenation increases from 0HC, 1HC, to 2HC. For example, the lattice constants are extended by 8–9%, 1–9%, and 0–10% for CrX$_2$, MoX$_2$, and WX$_2$, respectively, under hydrogenation.

Magnetic Properties.   Our calculations show that the hydrogenation results in the phase transition of TMD monolayers, which may also tune other physical properties. In this section, we focus on the effect of hydrogenation on the magnetic properties of the TMD monolayers. To find the magnetic ground state, a supercell with

Group VII	Structure	Conductivity	Magnetic state	Magnetic moment of M atom (μ_B)	Magnetic moments of X atom & X atom with H (μ_B)	Curie Temperature (K)	Exchange Energy (meV)
TcS$_2$	2H-0HC	metal	NM	—	—	—	0
	1T-1HC	metal	NM	—	—	—	0
	1T-2HC	half-metal	FM	0.94	0.002	541	70
TcSe$_2$	2H-0HC	metal	NM	—	—	—	1
	1T-1HC	half-metal	FM	1.66	0.052 & 0.045	613	80
	1T-2HC	half-metal	FM	0.88	0.012	117	15
TcTe$_2$	2H-0HC	metal	NM	—	—	—	4
	1T-1HC	metal	NM	—	—	—	6
	1T-2HC	metal	PM	0.61	0.004	—	−2
ReS$_2$	2H-0HC	metal	NM	—	—	—	2
	1T-1HC	metal	NM	—	—	—	0
	1T-2HC	half-metal	FM	0.89	0.001	454	59
ReSe$_2$	2H-0HC	metal	NM	—	—	—	4
	1T-1HC	half-metal	FM	1.51	0.051 & 0.036	537	69
	1T-2HC	half-metal	FM	0.84	0.009	204	26
ReTe$_2$	2H-0HC	metal	NM	—	—	—	1
	1T-1HC	metal	NM	—	—	—	1
	1T-2HC	metal	NM	—	—	—	−3

Table 4. Electronic, and magnetic ground states and magnetic moments of MX$_2$-nHC (n = 0, 1, and 2). Non-magnetism, paramagnetism, ferromagnetism, and anti-ferromagnetism are denoted as NM, PM, FM and AFM, respectively.

$2 \times 2 \times 1$ unit cells for each MX$_2$ system is constructed (referred as 221 supercell in Supporting Data S1). As an indication of stable ground state, the exchange energy (E$_{ex}$) is calculated as below:

$$E_{ex} = (E_{AFM} - E_{FM})/N \qquad (2)$$

where E$_{AFM}$ and E$_{FM}$ are the total energies of a MX$_2$ monolayer at antiferromagnetic and ferromagnetic states, respectively, and N is the number of unit cells adopted in calculation (N = 4 in a 221 supercell). The MX$_2$ monolayer is ferromagnetic (FM) when E$_{ex}$ is positive, while antiferromagnetic (AFM) when E$_{ex}$ is negative. We consider the systems as non-magnetism (NM) when the absolute values of E$_{ex}$, E$_{AFM}$ − E$_{NM}$, and E$_{FM}$ − E$_{NM}$ are less than 10 meV per unit cell because of possible calculation error.

The calculated exchange energies show that nonmagnetic TiX$_2$, ZrS$_2$ and ZrSe$_2$ monolayers switch to ferromagnetic, then back to nonmagnetic as the hydrogenation progresses from 0HC, 1HC, to 2HC (Fig. 3a). Whereas, ZrTe$_2$ and HfX$_2$ monolayers are nonmagnetic regardless of the hydrogenation. The Curie temperatures (T$_C$) of ferromagnetic systems can be estimated from K$_B$T$_C$ = (2/3)E$_{ex}$ based on the mean field theory and Heisenberg model[46], which are 448, 297, 149, 90, and 91 K for TiTe$_2$-1HC, TiSe$_2$-1HC, TiS$_2$-1HC, ZrS$_2$-1HC and ZrSe$_2$-1HC, respectively (Table 2).

For MX$_2$ monolayers with M from group VI, the magnetic switching under hydrogenation is slightly complicated. CrS$_2$ and CrSe$_2$ switch following NM → AFM → FM with the hydrogenation increasing (Fig. 3b). CrTe$_2$-0HC and CrTe$_2$-1HC are antiferromagnetic, but CrTe$_2$-2HC is ferromagnetic. MX$_2$ (M = Mo and W) monolayers with and without hydrogenation are nonmagnetic, except MoTe$_2$-2HC and WTe$_2$-2HC are ferromagnetic because their exchange energies are positive (Fig. 3b) and 1T-MoSe$_2$-2HC is paramagnetic because the energies at its magnetic states are lower than that at non-magnetic state (Supporting data, Table S1). Importantly, the Curie temperatures of CeS$_2$-2HC, CrSe$_2$-2HC, MoTe$_2$-2HC, and WTe$_2$-2HC are above 1000 K (Table 3).

For MX$_2$ monolayers with M from VII, we see that MTe$_2$ (M = Tc and Re) are nonmagnetic regardless of hydrogenation (Fig. 3c), except 1T-TcTe$_2$-2HC is paramagnetic because its magnetic states are more stable than its non-magnetic state (Supporting Data, Table S1). For systematic study, Tc is considered although it is radioactive. MSe$_2$ switches from non-magnetism to ferromagnetism after hydrogenation. MS$_2$-0HC and MS$_2$-1HC are non-magnetic, while MS$_2$-2HC monolayers are ferromagnetic (Fig. 3c and Table 4). The Curie temperatures range from 117 to 613 K for ferromagnetic systems in this group.

For MX$_2$ with M from group X, NiS$_2$ and NiSe$_2$ show the same magnetic evolution as NM → FM → AFM with the hydrogenation increasing (0HC → 1HC → 2HC), whereas NiTe$_2$ is nonmagnetic regardless of hydrogenation (Fig. 3d and Table 5). The ground states of MS$_2$ and MSe$_2$ (M = Pd and Pt) switch as NM → FM → NM with the hydrogenation increasing (0HC → 1HC → 2HC). However, MTe$_2$ keeps NM unchanged under hydrogenation. The Curie temperatures of ferromagnetic systems in this group varies from 171 to 233 K.

Our calculations show that the hydrogenation induces not only the phase transitions of MX$_2$ monolayers, but magnetic switching. Among all 33 considered systems, CrS$_2$-2HC has the highest Tc (1317 K). The estimated Curie temperature needs to be confirmed experimentally. The ferromagnetic MX$_2$ systems with Tc above room temperature may find applications in spintronics. To reveal the origin of the magnetic switching, their electronic structures are calculated.

Group X	Condition	Conductivity	Magnetic state	Magnetic moment of M atom (μ_B)	Magnetic moments of X atom & X atom with H (μ_B)	Curie Temperature (K)	Exchange Energy (meV)
NiS$_2$	1T-0HC	semiconductor	NM	—	—	—	0
	1T-1HC	half-metal	FM	0.59	0.176 & 0.065	228	30
	1T-2HC	metal	AFM	1.04	0.067	—	−73
NiSe$_2$	1T-0HC	semiconductor	NM	—	—	—	0
	1T-1HC	semiconductor	FM	0.41	0.108 & 0.026	233	30
	1T-2HC	metal	AFM	0.51	0.011	—	−14
NiTe$_2$	1T-0HC	metal	NM	—	—	—	1
	1T-1HC	metal	NM	—	—	—	8
	1T-2HC	metal	NM	—	—	—	8
PdS$_2$	1T-0HC	semiconductor	NM	—	—	—	0
	1T-1HC	semiconductor	FM	0.33	0.220 & 0.054	197	25
	1T-2HC	metal	NM	—	—	—	0
PdSe$_2$	1T-0HC	semiconductor	NM	—	—	—	0
	1T-1HC	semiconductor	FM	0.24	0.170 & 0.031	171	22
	1T-2HC	metal	NM	—	—	—	0
PdTe$_2$	1T-0HC	semiconductor	NM	—	—	—	0
	1T-1HC	metal	NM	—	—	—	2
	1T-2HC	metal	NM	—	—	—	0
PtS$_2$	1T-0HC	semiconductor	NM	—	—	—	0
	1T-1HC	semiconductor	FM	0.29	0.146 & 0.040	195	25
	1T-2HC	metal	NM	—	—	—	0
PtSe$_2$	1T-0HC	semiconductor	NM	—	—	—	0
	1T-1HC	semiconductor	FM	0.29	0.146 & 0.040	195	25
	1T-2HC	metal	NM	—	—	—	0
PtTe$_2$	1T-0HC	semiconductor	NM	—	—	—	0
	1T-1HC	metal	NM	—	—	—	1
	1T-2HC	metal	NM	—	—	—	0

Table 5. Electronic, and magnetic ground states and magnetic moments of MX$_2$-nHC (n = 0, 1, and 2 & M is from group X). Non-magnetism, ferromagnetism, and anti-ferromagnetism are denoted as NM, FM and AFM, respectively.

Electronic Properties. To understand the magnetic evolution of MX$_2$ monolayers under hydrogenation, the electronic structures and magnetic moments of MX$_2$ monolayers with and without hydrogenation are calculated (Figs 4 and 7, S2~S12, and Tables 2~5). The calculated partial density of states (PDOSs) of TiX$_2$-nHC show that nonmagnetic TiX$_2$-0HC and TiX$_2$-2HC monolayers are either metallic or semiconducting (Figs 4a,c and S2a,c), while ferromagnetic TiS$_2$-1HC and TiSe$_2$-1HC monolayers are n-type semiconductors and TiTe$_2$-1HC is narrow band semiconductor (Figs 4b,e,h and S2b,e,h). The d electrons of Ti atoms near the Fermi levels are spin-polarized (Fig. 4b,e,h), leading to the magnetic moments of 0.46, 0.62, and 0.71 μ_B/Ti in TiX$_2$-1HC (X = S, Se, and Te), respectively (Table 2). The p electrons of X atoms in TiX$_2$-1HC are also weakly spin-polarized (Fig. 4b,e,h), leading to smaller magnetic moments (Table 2), which are anti-parallel to the moments of Ti atoms. Therefore, the ferromagnetism of TiX$_2$-1HC may attribute to the double-exchange[11,14,47–50]. Pure ZrS$_2$ and ZrSe$_2$ monolayers are semiconductors and their band gaps are reduced by two-surface hydrogenation (S3). The ferromagnetic ZrS$_2$-1HC and ZrSe$_2$-1HC are half-metal (S3b,e). Nonmagnetic ZrTe$_2$ switches from metal, n-type semiconductor, to intrinsic semiconductor as hydrogenation increases from 0HC, 1HC, and 2HC (S3g–i). Pure nonmagnetic HfS$_2$ and HfSe$_2$ monolayers are semiconductors, and switch to metal upon hydrogenation (S4b,c,e,f), except that HfS$_2$-2HC is narrow-band semiconductor (S4c). Nonmagnetic HfTe$_2$ monolayer keeps metallic regardless of hydrogenation (S4g,h,i).

For MX$_2$ with M from group VI, accompanying with the magnetic switching of NM → AFM → FM, the electronic properties of CrX$_2$ monolayers switch from semiconductor, metal, to half-metal as hydrogenation increases (0HC → 1HC → 2HC) (Figs 5 and S5). Nonmagnetic MoX$_2$ (X = S and Se) systems switch from intrinsic semiconductor, n-type semiconductor, to metal as hydrogenation increases (S6a–f). Semiconducting MoTe$_2$ monolayer transfers to metal upon 1HC, and to half-metal upon 2HC (S6g–i). WX$_2$ monolayers show the same electronic switching as MoX$_2$ upon hydrogenation (S7).

For MX$_2$ with M from group VII, nonmagnetic TcS$_2$-0HC and TcS$_2$-1HC are metallic, and ferromagnetic TcS$_2$-2HC is half-metallic (Figs 6a–c and S8). Nonmagnetic TcSe$_2$-0HC is metal (Fig. 6d) and ferromagnetic TcSe$_2$-1HC and TcSe$_2$-2HC are half-metals, respectively (Fig. 6e,f). Nonmagnetic TcTe$_2$ monolayers with and without hydrogenation are metallic (Figs 6g–i and S8). The nonmagnetic ReX$_2$ monolayers with and without hydrogenation are metallic (S9a,b,d,g–i), while ferromagnetic counterparts are half-metallic (S9c,e,f).

For MX$_2$ with M from group X, semiconducting NiX$_2$ (X = S and Se) monolayers switch to half-metal upon 1HC (Figs 7b,e and S10b,e), and metallic upon 2HC (Figs 7c,f and S10c,f). Nonmagnetic NiTe$_2$ systems keep
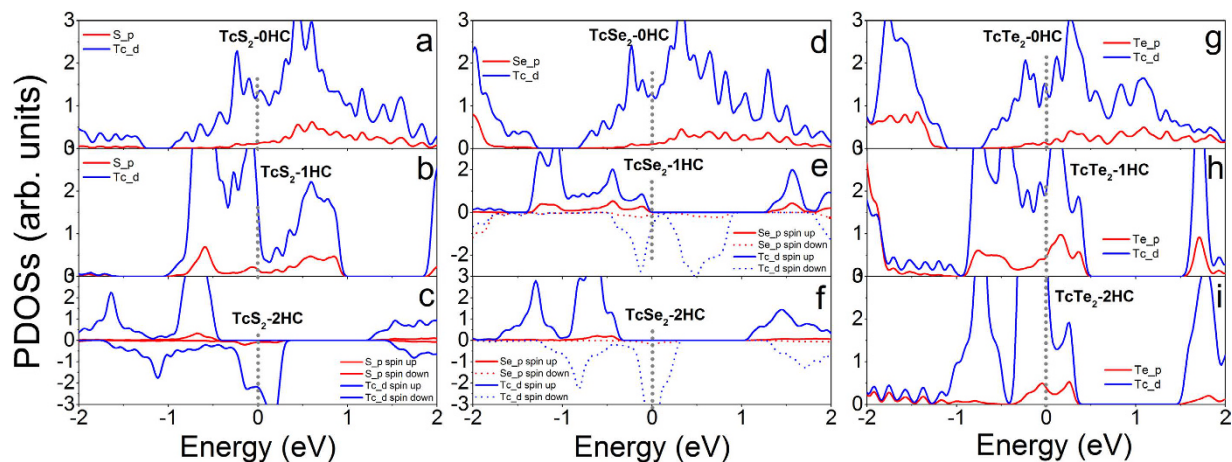
Figure 6. Calculated partial density of states of (**a**) TcS_2-0HC, (**b**) TcS_2-1HC, (**c**) TcS_2- 2HC, (**d**) $TcSe_2$-0HC, (**e**) $TcSe_2$-1HC, (**f**) $TcSe_2$-2HC, (**g**) $TcTe_2$-0HC, (**h**) $TcTe_2$-1HC and (**i**) $TcTe_2$-2HC monolayers. The Fermi level is at 0 eV and indicated with gray dotted line.
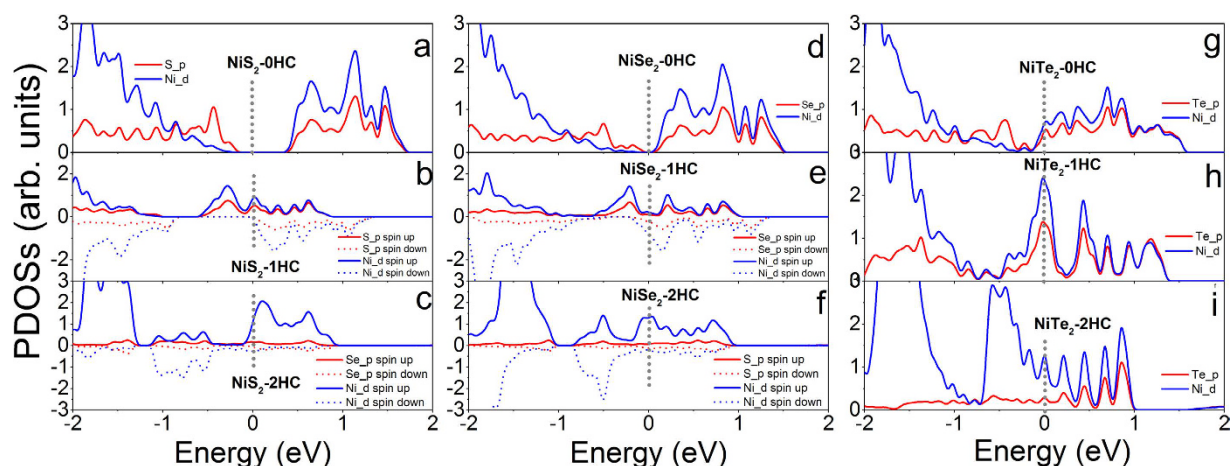
**Figure 7.** Calculated partial density of states of (**a**) NiS_2-0HC, (**b**) NiS_2-1HC, (**c**) NiS_2- 2HC, (**d**) $NiSe_2$-0HC, (**e**) $NiSe_2$-1HC, (**f**) $NiSe_2$-2HC, (**g**) $NiTe_2$-0HC, (**h**) $NiTe_2$-1HC and (**i**) $NiTe_2$-2HC monolayers. The Fermi level is at 0 eV and indicated with gray dotted line.

metallic regardless of hydrogenation (Figs 7g–i and S10 g–i). Nonmagnetic MX_2-0HC and MX_2-2HC monolayers (M = Pd and Pt, X = S and Se) are semiconducting and metallic, respectively (S12a,c,d,f, and S13a,c,d,f), and MX_2-1HC monolayers are ferromagnetic n-type semiconductors (S11b,e and S12b,e).

The calculated electronic properties clearly show that metallic or semiconducting systems are nonmagnetic/antiferromagnetic, and half metallic or doped semiconducting systems are ferromagnetic. The ferromagnetism is contributed to the carrier-mediated double exchange[11,24,47–50].

Catalytic Ability for Hydrogen Evolution. MX_2 monolayers have been widely investigated as electrocatalysts for hydrogen evolution reaction (HER)[25,26,32–34,42–44,51–60]. In this section, we investigate the catalytic activities of the considered 33 MX_2 systems. To characterize their catalytic performances, Gibbs free energies (ΔG_H) are calculated based on published methods[43,53,54,60]. A catalyst with optimal performance needs to have near-zero ΔG_H. Two HER processes, individual and collective processes, are considered. I-ΔG_H and A-ΔG_H are referred as the Gibbs free energies calculated from individual and collective processes, respectively[26,53]. To investigate the catalytic activities of the 33 MX_2 monolayers in HER, a supercell with $3 \times 3 \times 1$ unit cells for each MX_2-1HC monolayer, referred as 331 supercell, is constructed (S13). Hydrogen atoms are taken away one by one from 331 supercell to calculate the Gibbs free energies, where the partial hydrogen coverages is referred as $\frac{n}{9}$ (n = 1–9). Both 1T and 2H phases are considered because of the possible phase transition as discussed above.

Out of 33 MX_2 monolayers, we find that TiS_2 monolayer shows excellent catalytic ability at a wide range of hydrogen coverages. Our calculations show that both I-ΔG_H and A-ΔG_H of TiS_2-1HC increase with the increment of hydrogen coverages (Fig. 8a–d), which are much closer to zero than those of $TiSe_2$ and $TiTe_2$ at the same hydrogen coverages, similar to VX_2 monolayers[25]. Interestingly, we see that 2H phase shows much better catalytic performance than 1T phase because of the relatively lower overpotentials (absolute value of Gibbs free energy) at
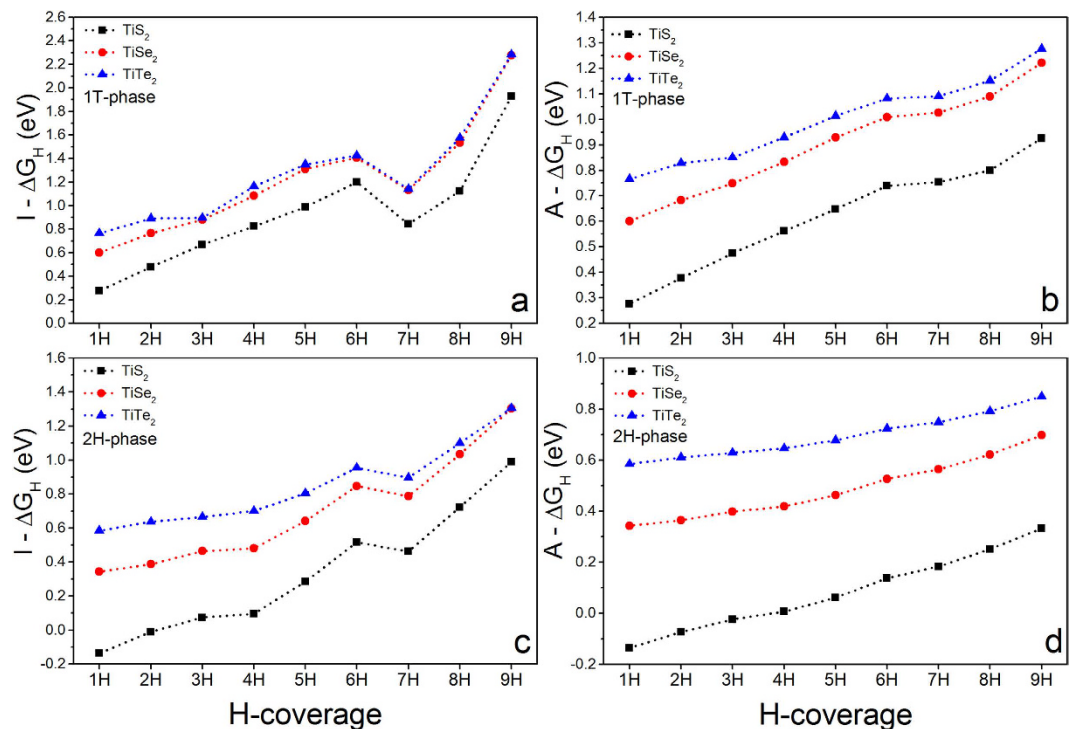
Figure 8. Calculated Gibbs free energies of TiS$_2$ monolayer as a function of one-surface hydrogen coverages in 1T phase: (**a**) I-ΔG$_H$, and (**b**) A-ΔG$_H$, in 2H phase: (**c**) I-ΔG$_H$, and (**d**) A-ΔG$_H$.

the same hydrogen coverages. As discussed above, 1T phase of pure TiX$_2$ is more stable than its 2H phase, indicating that the metastable phase shows better catalytic performance, which is similar to MoS$_2$ and WS$_2$ monolayers[30,32,33]. At the same time, we showed above that the phase transition from 1T to 2H can be easily realized through surface hydrogenation. Therefore, 2H-TiX$_2$ could be achieved and stabilized during the process of HER. Importantly, I-ΔG$_H$ of 2H-TiS$_2$ is close-to-zero (-0.14, -0.01, 0.07, and 0.09 eV) in a hydrogen coverage ranging from $\frac{1}{9}$ to $\frac{4}{9}$ in the individual process. For collective process, A-ΔG$_H$ (-0.14, -0.07, -0.02, 0.006, and 0.06 eV) is near-zero in a hydrogen density of from $\frac{1}{9}$ to $\frac{5}{9}$. The near-zero Gibbs free energies clearly indicate that 2H-TiS$_2$ monolayer show high catalytic ability within a wide range of hydrogen coverages. The catalytic activity of 2H-TiS$_2$ monolayer is much better than other MX$_2$ that only showed catalytic activity at certain hydrogen coverage. For example, VS$_2$ monolayer was good at low-hydrogen coverages[25]. The Mo-edge of MoS$_2$ was only catalytically active with an A-ΔG$_H$ of 0.06 eV at a hydrogen density of $\frac{2}{4}$[44]. 1T-WS$_2$ monolayer has an I-ΔG$_H$ of 0.28 eV at a hydrogen density of $\frac{1}{16}$[30]. Therefore, TiS$_2$ monolayer possesses overall excellent catalytic ability, which is comparable to Pt, due to near-zero ΔG$_H$ in wide range of hydrogen densities.

Conclusions

In summary, we present a comprehensive first-principles calculations on the physical and chemical properties of 2D TMDs with and without hydrogenation. We find that the hydrogenation plays an important role on tuning the structural, electronic, magnetic and catalytic properties of TMD monolayers (Fig. 9). We show that pure 1T-MX$_2$ (M in group IV) monolayers transfer into 2H phase upon hydrogenation, their ground states can be tuned from non-magnetic to ferromagnetic accompanying with electronic switching from semiconducting to half-metallic. Phase transition between 1T and 2H phases in MX$_2$ (M is from group VI and VII), and magnetic and electronic switching in MX$_2$ (M is from group VI, VII, X) can be realized by the hydrogenation. We further predict that 2H-TiS$_2$ monolayer, out of 33 MX$_2$ monolayers, has excellent catalytic ability in a wide range of hydrogen coverage and may find applications as electrocatalyst in hydrogen evolution reaction. It is expected that MX$_2$ monolayers with controllable structure, tunable electronic, magnetic and optimized catalytic properties can find applications in catalysts, spintronics, sensors and nanodevices.

Methods

The first-principles calculations are conducted to systematically investigate the structural, electronic and magnetic properties of 2D TMDs monolayers through hydrogenation as well as their catalytic ability in hydrogen evolution reduction. Based on the density functional theory (DFT)[61] and the Perdew-Burke-Eznerhof generalized gradient approximation (PBE-GGA)[62], our calculations are carried out by using the Vienna ab initio simulation package (VASP)[63], which is incorporated with projector augmented wave (PAW) scheme[64,65]. An energy cut-off of 500 eV is consistently used in our calculations. Large vacuum regions of 20 Å along vertical directions are used in constructing the unit cells to avoid interaction between neighboring monolayers. The integration over the first Brillouin
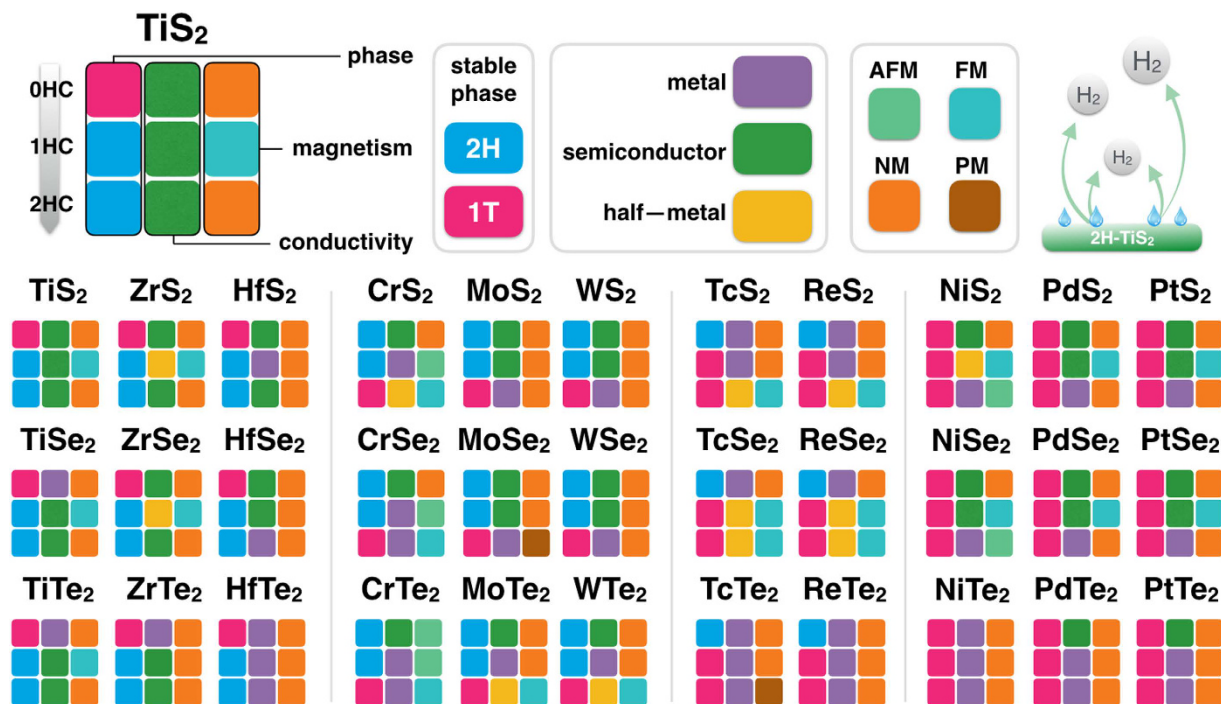
Figure 9. Summary of our findings on the structural, magnetic, electronic and catalytic properties of 33 TMDs monolayers with and without hydrogenation.

zone is based on the Monkhorst and Pack scheme of k-point sampling[66]. The $13 \times 13 \times 1$ grid, $5 \times 5 \times 1$ grid, and $3 \times 3 \times 1$ grid for k-point sampling are used for geometry relaxation of unit cells, $2 \times 2 \times 1$ supercells, and $3 \times 3 \times 1$ supercells, respectively. Spin-polarized calculations are also employed to study the magnetic properties. Good Convergence is obtained with these parameters and the total energy is converged to 2.0×10^{-5} eV/atom.

The Gibbs free energy is an important descriptor for electrocatalyst in HER, and can be calculated as $\Delta G_H = \Delta E_H + \Delta E_{ZPE} - T \Delta S_H$, where ΔE_H is the hydrogen chemisorption energy defined as I-$\Delta E_H = E(MX_2 + mH) - E(MX_2 + (m-1)H) - E(H_2)/2$ for individual process and A-$\Delta E_H = [E(MX_2 + mH) - E(MX_2) - mE(H_2)/2]/m$ for average process, respectively. $E(H_2)$, $E(MX_2)$ and $E(MX_2 + mH)$ are the calculated total energies of a hydrogen molecule, pure MX_2 and hydrogenated MX_2, m is the number of hydrogen atoms adsorbed on a monolayer. ΔE_{ZPE} is the difference in zero point energy between the adsorbed and the gas phase, ΔS_H is the difference in entropy, $\Delta E_{ZPE} - T \Delta S_H$ is about 0.24 eV[25,42–45,53]. Therefore, Gibbs free energy can be calculated as $\Delta G_H = \Delta E_H + 0.24$. Positive ΔG_H of a catalyst suggests weak adsorption of protons, leading to absorbing less protons on its surface, however, negative ΔG_H indicates strong binding of protons on a catalyst's surface, resulting in difficult desorption. Electrocatalysts with neutral-thermal (close-to-zero) ΔG_H exhibit optimal catalytic ability in hydrogen evolution with neither strong nor weak binding of protons in the electrolyte.

References

1. Wang, Q. H., Kalantar-Zadeh, K., Kis, A., Coleman, J. N. & Strano, M. S. Electronics and optoelectronics of two-dimensional transition metal dichalcogenides. *Nat. Nanotechnol.* **7,** 699–712 (2012).
2. Chhowalla, M. *et al.* The chemistry of two-dimensional layered transition metal dichalcogenide nanosheets. *Nat. Chem.* **5,** 263–275 (2013).
3. Lin, C. *et al.* Hydrogen-incorporated TiS₂ ultrathin nanosheets with ultrahigh conductivity for stamp-transferrable electrodes. *J. Am. Chem. Soc.* **135,** 5144–5151 (2013).
4. Liu, W. *et al.* Role of metal contacts in designing high-performance monolayer n-type WSe₂ field effect transistors. *Nano Lett.* **13,** 1983–1990 (2013).
5. Radisavljevic, B., Radenovic, A., Brivio, J., Giacometti, V. & Kis, A. Single-layer MoS₂ transistors. *Nat. Nanotechnol.* **6,** 147–150 (2011).
6. Li, H., Shi, Y., Chiu, M.-H. & Li, L.-J. Emerging energy applications of two-dimensional layered transition metal dichalcogenides. *Nano Energy* **18,** 293–305 (2015).
7. Ding, Y. *et al.* First principles study of structural, vibrational and electronic properties of graphene-like MX₂ (M = Mo, Nb, W, Ta; X = S, Se, Te) monolayers. *Phys. B: Condensed Matter* **406,** 2254–2260 (2011).
8. Feng, J. *et al.* Metallic few-layered VS₂ ultrathin nanosheets: High two-dimensional conductivity for in-plane supercapacitors. *J. Am. Chem. Soc.* **133,** 17832–17838 (2011).
9. Ma, Y. *et al.* Evidence of the existence of magnetism in pristine VX₂ monolayers (X = S, Se) and their strain-induced tunable magnetic properties. *ACS Nano* **6,** 1695–1701 (2012).
10. Li, F., Tu, K. & Chen, Z. Versatile electronic properties of VSe₂ bulk, few-layers, monolayer, nanoribbons, and nanotubes: A computational exploration. *J. Phys. Chem. C* **118,** 21264–21274 (2014).
11. Pan, H. Magnetic and electronic evolutions of hydrogenated VTe₂ monolayer under tension. *Sci. Rep.* **4,** 7524 (2014).
12. Jing, Y., Zhou, Z., Cabrera, C. R. & Chen, Z. Metallic VS₂ monolayer: A promising 2D anode material for lithium ion batteries. *J. Phys. Chem. C* **117,** 25409–25413 (2013).

13. Huo, N. *et al.* Photoresponsive and gas sensing field-effect transistors based on multilayer WS$_2$ Nanoflakes. *Sci. Rep.* **4,** 5209 (2014).
14. Song, X., Hu, J. & Zeng, H. Two-dimensional semiconductors: Recent progress and future perspectives. *J. Mater. Chem. C* **1,** 2952–2969 (2013).
15. Loh, T. A. J., Chua, D. H. C. & Wee, A. T. S. One-step synthesis of few-layer WS$_2$ by pulsed laser deposition. *Sci. Rep.* **5,** 18116 (2015).
16. Shi, Y., Li, H. & Li, L.-J. Recent advances in controlled synthesis of two-dimensional transition metal dichalcogenides via vapour deposition techniques. *Chem. Soc. Rev.* **44,** 2744–2756 (2015).
17. Tan, C. & Zhang, H. Wet-chemical synthesis and applications of non-layer structured two-dimensional nanomaterials. *Nat. Commun.* **6,** 7873 (2015).
18. Zhang, X. & Xie, Y. Recent advances in free-standing two-dimensional crystals with atomic thickness: Design, assembly and transfer strategies. *Chem. Soc. Rev.* **42,** 8187–8199 (2013).
19. Voiry, D., Mohite, A. & Chhowalla, M. Phase engineering of transition metal dichalcogenides. *Chem. Soc. Rev.* **44,** 2702–2712 (2015).
20. Voiry, D. *et al.* Covalent functionalization of monolayered transition metal dichalcogenides by phase engineering. *Nat. Chem.* **7,** 45–49 (2014).
21. Zhang, H., Liu, L.-M. & Lau, W.-M. Dimension-dependent phase transition and magnetic properties of VS$_2$. *J. Mater. Chem. A* **1,** 10821–10828 (2013).
22. Zhou, Y. *et al.* Tensile strain switched Ferromagnetism in layered NbS$_2$ and NbSe$_2$. *ACS Nano* **6,** 9727–9736 (2012).
23. Shi, H., Pan, H., Zhang, Y.-W. & Yakobson, B. I. Strong ferromagnetism in hydrogenated monolayer MoS$_2$ tuned by strain. *Phys. Rev. B* **88,** 205305 (2013).
24. Pan, H. Electronic and magnetic properties of vanadium dichalcogenides monolayers tuned by hydrogenation. *J. Phys. Chem. C* **118,** 13248–13253 (2014).
25. Pan, H. Metal dichalcogenides monolayers: Novel catalysts for electrochemical hydrogen production. *Sci. Rep.* **4,** 5348 (2014).
26. Pan, H. Tension-enhanced hydrogen evolution reaction on vanadium disulfide monolayer. *Nanoscale Res. Lett.* **11,** 113 (2016).
27. Wang, H. *et al.* Electrochemical tuning of vertically aligned MoS$_2$ nanofilms and its application in improving hydrogen evolution reaction. *Pro. Natl. Acad. Sci.* **110,** 19701–19706 (2013).
28. Tang, Q. & Jiang, D. Stabilization and band-gap tuning of the 1T-MoS$_2$ monolayer by covalent functionalization. *Chem. Mater.* **27,** 3743–3748 (2015).
29. Lu, P., Wu, X., Guo, W. & Zeng, X. C. Strain-dependent electronic and magnetic properties of MoS$_2$ monolayer, bilayer, nanoribbons and nanotubes. *Phys. Chem. Chem. Phys.* **14,** 13035–13040 (2012).
30. Voiry, D. *et al.* Enhanced catalytic activity in strained chemically exfoliated WS$_2$ nanosheets for hydrogen evolution. *Nat. Mater.* **12,** 850–855 (2013).
31. Yang, C.-Y. *et al.* Phase-driven magneto-electrical characteristics of single-layer MoS$_2$. *Nanoscale* **8,** 5627–5633 (2016).
32. Lukowski, M. A. *et al.* Enhanced hydrogen evolution catalysis from chemically exfoliated metallic MoS$_2$ Nanosheets. *J. Am. Chem. Soc.* **135,** 10274–10277 (2013).
33. Geng, X. *et al.* Pure and stable metallic phase molybdenum disulfide nanosheets for hydrogen evolution reaction. *Nat. Commun.* **7,** 10672 (2016).
34. Morales-Guio, C. G., Stern, L.-A. & Hu, X. Nanostructured hydrotreating catalysts for electrochemical hydrogen evolution. *Chem. Soc. Rev.* **43,** 6555–6569 (2014).
35. Eda, G. *et al.* Coherent atomic and electronic heterostructures of single-layer MoS$_2$. *ACS Nano* **6,** 7311–7317 (2012).
36. Voiry, D. *et al.* Conducting MoS$_2$ nanosheets as catalysts for hydrogen evolution reaction. *Nano Lett.* **13,** 6222–6227 (2013).
37. Ambrosi, A., Sofer, Z. & Pumera, M. 2H → 1T phase transition and hydrogen evolution activity of MoS$_2$, MoSe$_2$, WS$_2$ and WSe$_2$ strongly depends on the MX$_2$ composition. *Chem. Commun.* **51,** 8450–8453 (2015).
38. Chou, S. S. *et al.* Understanding catalysis in a multiphasic two-dimensional transition metal dichalcogenide. *Nat. Commun.* **6,** 8311 (2015).
39. Tang, Q. & Jiang, D. Mechanism of hydrogen evolution reaction on 1T-MoS$_2$ from First principles. *ACS Catal.* **6,** 4953–4961 (2016).
40. Qu, Y., Pan, H., Kwok, C. T. & Wang, Z. Effect of doping on hydrogen evolution reaction of vanadium disulfide monolayer. *Nanoscale Res. Lett.* **10,** 480 (2015).
41. Koh, E. W. K., Chiu, C. H., Lim, Y. K., Zhang, Y.-W. & Pan, H. Hydrogen adsorption on and diffusion through MoS$_2$ monolayer: First-principles study. *Int. J. Hydrog. Energy* **37,** 14323–14328 (2012).
42. Wang, H. *et al.* Transition-metal doped edge sites in vertically aligned MoS$_2$ catalysts for enhanced hydrogen evolution. *Nano Research* **8,** 566–575 (2015).
43. Tsai, C., Chan, K., Nørskov, J. K. & Abild-Pedersen, F. Rational design of MoS$_2$ catalysts: Tuning the structure and activity via transition metal doping. *Catal. Sci. Technol.* **5,** 246–253 (2015).
44. Tsai, C., Chan, K., Abild-Pedersen, F. & Nørskov, J. K. Active edge sites in MoSe$_2$ and WSe$_2$ catalysts for the hydrogen evolution reaction: A density functional study. *Phys. Chem. Chem. Phys.* **16,** 13156–13164 (2014).
45. Pandey, M., Vojvodic, A., Thygesen, K. S. & Jacobsen, K. W. Two-dimensional metal dichalcogenides and oxides for hydrogen evolution: A computational screening approach. *J. Phys. Chem. Lett.* **6,** 1577–1585 (2015).
46. Kudrnovský, J. *et al.* Exchange interactions in III-V and group-IV diluted magnetic semiconductors. *Phys. Rev. B* **69,** 115208 (2004).
47. Anderson, P. W. Antiferromagnetism. Theory of Superexchange Interaction. *Phys. Rev.* **79,** 350–356 (1950).
48. Panda, S. K., Dasgupta, I., Sasioglu, E., Blugel, S. & Sarma, D. D. NiS - An unusual self-doped, nearly compensated antiferromagnetic metal. *Sci. Rep.* **3,** 2995 (2013).
49. Akai, A. Ferromagnetism and its stability in the diluted magnetic semiconductor (In, Mn) As. *Phys. Rev. Lett.* **81,** 3002–3005 (1998).
50. Dalpian, G. M. & Wei, S. H. Carrier-mediated stabilization of ferromagnetism in semiconductors: holes and electrons. *Phys. Stat. Sol. (b)* **243,** 2170–2187 (2006).
51. Liao, T., Sun, Z., Sun, C., Dou, S. X. & Searles, D. J. Electronic coupling and catalytic effect on H$_2$ evolution of MoS$_2$/graphene nanocatalyst. *Sci. Rep.* **4,** 6256 (2014).
52. Dong, H. *et al.* Three-dimensional nitrogen-doped graphene supported molybdenum disulfide nanoparticles as an advanced catalyst for hydrogen evolution reaction. *Sci. Rep.* **5,** 17542 (2015).
53. Qu, Y., Pan, H., Tat Kwok, C. & Wang, Z. A first-principles study on the hydrogen evolution reaction of VS$_2$ nanoribbons. *Phys. Chem. Chem. Phys.* **17,** 24820–24825 (2015).
54. Li, H. *et al.* Charge-transfer induced high efficient hydrogen evolution of MoS$_2$/graphene cocatalyst. *Sci. Rep.* **5,** 18730 (2015).
55. Gong, Q. *et al.* Ultrathin MoS$_{2(1-x)}$Se$_{2x}$ alloy Nanoflakes for Electrocatalytic hydrogen evolution reaction. *ACS Catal.* **5,** 2213–2219 (2015).
56. Kibsgaard, J., Chen, Z., Reinecke, B. N. & Jaramillo, T. F. Engineering the surface structure of MoS$_2$ to preferentially expose active edge sites for electrocatalysis. *Nat. Mater.* **11,** 963–969 (2012).
57. Jaramillo, T. F. *et al.* Identification of active edge sites for Electrochemical H$_2$ evolution from MoS$_2$ Nanocatalysts. *Science* **317,** 100–102 (2007).
58. Hinnemann, B. *et al.* Biomimetic hydrogen evolution: MoS$_2$ Nanoparticles as catalyst for hydrogen evolution. *Chem.Inform* **36,** 5308–5309 (2005).
59. Bollinger, M. V. *et al.* One-Dimensional metallic edge states in MoS$_2$. *Phys. Rev. Lett.* **87,** 196803 (2001).
60. Nørskov, J. K. *et al.* Trends in the exchange current for hydrogen evolution. *J. Electrochem. Soc.* **152,** J23–J26 (2005).

61. Hohenberg, P. & Kohn, W. Inhomogeneous electron gas. *Phys. Rev.* **136,** B864–B871 (1964).
62. Blöchl, P. E. Projector augmented-wave method. *Phys. Rev. B* **50,** 17953–17979 (1994).
63. Kresse, G. & Furthmüller, J. Efficient iterative schemes for ab initio total-energy calculations using a plane-wave basis set. *Phys. Rev. B* **54,** 11169–11186 (1996).
64. Kresse, G. & Joubert, D. From ultrasoft pseudopotentials to the projector augmented-wave method. *Phys. Rev. B* **59,** 1758–1775 (1999).
65. Perdew, J. P., Burke, K. & Ernzerhof, M. Generalized gradient approximation made simple. *Phys. Rev. Lett.* **77,** 3865–3868 (1996).
66. Monkhorst, H. J. & Pack, J. Special points for brillouin-zone integrations. *Phys. Rev. B* **13,** 5188–5192 (1976).

Acknowledgements

Author Contributions

H.P. conceived the idea, Y.Q. performed the calculations, H.P. and Y.Q. wrote the paper and all authors revised the paper.

Additional Information

Supplementary information accompanies this paper at http://www.nature.com/srep

Competing financial interests: The authors declare no competing financial interests.

How to cite this article: Qu, Y. *et al.* Hydrogenation-controlled phase transition on two-dimensional transition metal dichalcogenides and their unique physical and catalytic properties. *Sci. Rep.* **6**, 34186; doi: 10.1038/srep34186 (2016).